From Voxels to Prognosis: AI-Driven Quantitative Chest CT Analysis Forecasts ICU Requirements in 78 COVID-19 Cases

Rudolf Bumm (rudolf.bumm@ksgr.ch)
Department of Thoracic Surgery, Kantonsspital Graubünden, Chur, Switzerland;
Paolo Zaffino
Department of Experimental and Clinical Medicine, University “Magna Graecia” of Catanzaro, 88100 Catanzaro, Italy
Andras Lasso
Laboratory for Percutaneous Surgery, Queen's University, Kingston, Canada
Raúl San José Estépar
Department of Radiology, Brigham and Women's Hospital, Harvard Medical School, Boston, MA, USA
Steven Pieper
Isomics Inc, Cambridge, Massachusetts
Jakob Wasserthal
Clinic of Radiology & Nuclear Medicine, University Hospital Basel, Petersgraben 4, 4031 Basel, Switzerland
Maria Francesca Spadea
Institute of Biomedical Engineering, Karlsruhe Institute of Technology (KIT), 76131 Karlsruhe, Germany
Tsogyal Latshang
Department of Pneumonology, Kantonsspital Graubünden, Chur, Switzerland
Nadine Kawel-Böhm
Department of Radiology, Kantonsspital Graubünden, Chur, Switzerland
Adrian Wäckerlin
Department of Intensive Care Medicine, Kantonsspital Graubünden, Chur, Switzerland
Raphael Werner
Department of Thoracic Surgery, Kantonsspital Graubünden, Chur, Switzerland
Gabriela Hässig
Department of Thoracic Surgery, Kantonsspital Graubünden, Chur, Switzerland
Markus Furrer
Department of Thoracic Surgery, Kantonsspital Graubünden, Chur, Switzerland
Ron Kikinis
Department of Radiology, Brigham and Women's Hospital, Harvard Medical School, Boston, MA, USA;

Research Article

Keywords: Lung involvement, COVID-19, Intensive care unit (ICU) admission, Computer analysis, Radiological expert, Clinical decision-making

Posted Date: July 5th, 2023

DOI: https://doi.org/10.21203/rs.3.rs-3027617/v5

Abstract

Background: The aim of the current study was to investigate the distribution and extent of lung involvement in patients with COVID-19 with AI-supported, automated computer analysis and to assess the relationship between lung involvement and the need for intensive care unit (ICU) admission. A secondary aim was to compare the performance of computer analysis with the judgment of radiological experts.

Methods: A total of 81 patients from an open-source COVID database with confirmed COVID-19 infection were included in the study. Three patients were excluded. Lung involvement was assessed in 78 patients using computed tomography (CT) scans, and the extent of infiltration and collapse was quantified across various lung lobes and regions. The associations between lung involvement and ICU admission were analyzed. Additionally, the computer analysis of COVID-19 involvement was compared against a human rating provided by radiological experts.

Results: The results showed a higher degree of infiltration and collapse in the lower lobes compared to the upper lobes ($p < 0.05$) No significant difference was detected in the COVID-19-related involvement of the left and right lower lobes. The right middle lobe demonstrated lower involvement compared to the right lower lobes ($p < 0.05$). When examining the regions, significantly more COVID-19 involvement was found when comparing the posterior vs. the anterior halves of the lungs and the lower vs. the upper half of the lungs. Patients, who required ICU admission during their treatment exhibited significantly higher COVID-19 involvement in their lung parenchyma according to computer analysis, compared to patients who remained in general wards. Patients with more than 40% COVID-19 involvement were almost exclusively treated in intensive care. A high correlation was observed between computer detection of COVID-19 affections and expert rating by radiological experts.

Conclusion: The findings suggest that the extent of lung involvement, particularly in the lower lobes, dorsal lungs, and lower half of the lungs, may be associated with the need for ICU admission in patients with COVID-19. Computer analysis showed a high correlation with expert rating, highlighting its potential utility in clinical settings for assessing lung involvement. This information may help guide clinical decision-making and resource allocation during ongoing or future pandemics. Further studies with larger sample sizes are warranted to validate these findings.

Introduction

The COVID-19 pandemic is caused by the novel coronavirus 2 (SARS-CoV-2), which was first identified in December 2019 in Wuhan, China (1). The virus quickly became a global pandemic, with hundreds of millions of cases and almost seven million deaths worldwide (2), (3).

Chest CT imaging plays an important role in the diagnosis and management of COVID-19, particularly in cases where RT-PCR testing is not available or inconclusive (4), (5). CT imaging reveals characteristic

features of the disease, provides information for diagnosis and staging, and can also help to monitor disease progression and assess the response to treatment (6).

Automated analysis of COVID-19-related chest CT scans would be very desirable for a number of reasons. Most importantly, the infiltrations and consolidations could be expressed as affected volume and directly quantified. The distribution of affected tissue in the sides of the lungs, lobes, and lung regions could be analyzed. Automatic processing could help to reduce the workload of radiologists and other healthcare professionals, enabling them to focus on patient care and other important tasks. Automation also has the potential to be more consistent than manual review, if it can be shown to be robust to differences across multiple clinical sites. Open-source availability of all software components would enable identical computations on computer hardware around the world which would support future pandemic preparedness.

We recently developed a free and open-source software - LungCTAnalyzer (7) - for the medical imaging software 3D Slicer (8), (9). The software is using AI-tools for lung and lobe segmentation. It is designed specifically for the analysis of lung CT scans, offering a comprehensive set of tools for the segmentation, quantification, and visualization of lung structures. By leveraging the power of 3D Slicer and building upon its functionalities, LungCTAnalyzer provides a user-friendly interface and a robust set of features that streamline the process of lung image analysis for the detection of emphysema, normal lung tissue, infiltrated and collapsed parenchyma.

As an open-source COVID dataset with radiologist scores has been published (10), the present study aims to quantitatively analyze the data to determine the accordance of computer vs. human analysis in order to demonstrate the feasibility of computer analysis with LungCTAnalyzer and to elaborate on the existing differences in lung involvement between the severity-scored groups, to evaluate whether tissue affection in severe cases could be attributed to the side of lungs, lung regions or lung lobes and to predict patients requiring ICU-treatment.

Methods

Ethical statement

All ethical statements have been included in the dataset paper (10).

Patient Population and Open Source Dataset

The dataset used in this study has been recently published and expanded (10). In short, it includes data from 81 COVID-19 patients (diagnoses confirmed by positive RT-PCR tests), 50 during the first phase of COVID-pandemic between April 2020 and May 2021 and 31 during the second between December 2020 and May 2021. They underwent non-contrast chest CT scans at Azienda Ospedaliera Pugliese-Ciaccio (Catanzaro, Italy). These scans feature volume reconstructions with 0.3 to 1 mm slice thickness. The average age of the patients was 56 years, ranging from 20 to 83, and the male-to-female ratio was 42:39. Two distinct scanners were utilized at the clinical facility: Siemens Somatom Go. now (Siemens Healthineers GmbH, Erlangen, Germany) and Toshiba Aquilion ONE (Canon Medical System Europe B.V., Zoetermeer, The Netherlands). Among the patients, 81 underwent a single CT scan for diagnostic purposes, while 12 received additional scans for follow-up, resulting in a total of 93 CT volumes in the database. To facilitate data sharing and processing, the DICOM files were anonymized and converted into NRRD format (http://teem.sourceforge.net/nrrd/ (accessed on 15 February 2021)) using 3D Slicer (8). The image collection was conducted with approval from the Hospital Ethics Committee, "Prot. 308."

Visual Assessment

Primary findings regarding COVID-19 in CT images involve atypical pneumonia and encompass two macroscopic lung tissue abnormalities: ground-glass opacity (GGO), which is an area of increased X-ray attenuation in the lung with preserved bronchial and vascular markings, and consolidation, referring to the filling of the pulmonary tree with material that attenuates X-rays more than the surrounding lung parenchyma.
An expert radiologist, (A.M, one of the authors of the dataset paper (10)), (with over 20 years of experience) was tasked with visually evaluating the CT images and assigning a clinical score, based on the extent of lung involvement with the aforementioned manifestations. The radiologist navigated through the volume on his radiological workstation in axial, sagittal, and coronal planes, assigning a lung involvement classification scale ranging from 0, indicating no lung involvement (0%), to 5, representing severe lung involvement (greater than 75%), with intermediate levels covering minimal (less than 5%), mild (5% to 25%), moderate (26% to 50%), and significant (51% to 75%) involvement. This took about two to three minutes per case. These scores are included in the open dataset alongside each image volume.

In an effort to appraise the potential for interobserver bias through a comparison between human evaluators, a second radiological specialist (N.K.B, a co-author of this study) undertook an independent visual assessment using an identical scoring system. Intriguingly, out of the 81 patients evaluated, she

deemed three as "not classifiable" (one patient with incomplete CT and two patients with pneumothorax). In addition, she noted three patients with possible preexisting lung disease.

We made a deliberate decision to exclude the three unclassifiably patients from the study and to retain the other three patients with possible lung disease in the dataset for the sake of providing a comprehensive reference.

Automated Segmentation of the Lungs and Lung Pathologies

This study employed an automated approach for the segmentation of the lungs and lung pathologies using the free and open-source medical imaging software 3D Slicer (8), for which we wrote a special extension in the programming language Python: LungCTAnalyzer (7) using the same software license. The program can be run in batch processing mode, without manual interaction. CT data were imported into 3D Slicer as NRRD files.

Data calibration

During a preliminary scan of all datasets, it became evident that the CT scans exhibited some heterogeneity in HU range, quality, windowing, and the presence of artifacts. Utilizing the TotalSegmentator (nnU-Net) (11) for segmentation, we were able to automatically generate segments corresponding to the trachea and the left erector spinae muscle in the CT datasets. We then evaluated the median Hounsfield units (HU) of both segmented structures in both scanners (Toshiba: Trachea: -931.6 Muscle: 22.68 [mean HU], Siemens: Trachea: -958.2 Muscle: 24.25 [mean HU]). A Python function then standardized CT scans by calibrating Hounsfield unit (HU) values for air and muscle. It takes a 3D numpy array (12), mean HU values for air and muscle, and returns a standardized CT scan. The function calculates a linear transformation to map input HU values to desired output values (-1000 HU for air, 30 HU for muscle, Figure 6). For the Toshiba scanner, we found a mean slope of 1.08 (Std Dev 0.06) and a mean intercept of 5.72 (Std Dev 16.46). For the Siemens scanner, we found a mean slope of 1.06 (Std Dev 0.06) and a mean intercept of 5.12 (Std Dev 16.98). The transformation is applied, and the adjusted CT scan is returned for further analysis. This calibration is intended to ensure consistency across datasets and facilitate further analysis.

Lung and lobe segmentation

Next, the segmentation process began using the Lung CT Segmenter (LCTS) module. Trachea, left iliopsoas muscle, lungs, and lobes were segmented involving the 3D Slicer TotalSegmentator (11) extension (13), which involves a tool for robust segmentation of 104 important anatomical structures in CT images with a well-trained neural network: nnU-Net (14). Mean radiodensity in Hounsfield Units (HU) of the trachea and iliopsoas muscle was automatically calculated (see above) for radiodensity evaluation. Each lung and lobe segmentation took about 114 s on the computer system described below.

Lung analysis segmentation

The calibrated scalar volume was then loaded into LungCTAnalyzer and lung analysis segments were generated for emphysema (-2000 to -950 HU), normal lung (-950 to -750 HU), infiltrated lung/GGO (-750 to -400 HU), collapsed lung (-400 to 0 HU), and vessels (> 0 HU). The volume of each of these segments was expressed in mm^3. These segments were created for each lung, lobe, and the upper and lower half of each lung, as well as the anterior and posterior halves of each lung. To accomplish that, we calculated the centroid for each segmented lung and constructed a matching quadrant of markups which was then used to crop away the posterior half of the lung if the anterior half was to be preserved (and vice versa). The same technique was used for isolating the upper and lower half of each lung.

Thresholds were not changed throughout the complete study. Each lung analysis segmentation took 187 s.

The complete analysis of 78 datasets takes ((114 + 187) * 78) / 60 = 391.3 minutes ~ 5 minutes per case. This includes data loading and saving.

Percentage of COVID-affected Lung

The 3D Slicer Segment Statistics tool was employed to analyze all generated lung structures and pathologies. The percentage of affected areas within both lungs, individual lungs, all lobes, and regions of interest were evaluated using the following formula:

PercentAffected = ((InfiltratedVolume_ml + CollapsedVolume_ml) * 100) / OrganVolume_ml

Vessel volumes were excluded from the total volumes, while airways were not considered. Ultimately, the findings were recorded in a CSV text file for further analysis and interpretation.

All processing was performed on the following system:

- Device: DESKTOP Windows 11
- Processor: 11th Gen Intel(R) Core(TM) i7-11700F @ 2.50GHz, 2.50 GHZ
- Installed RAM: 32.0 GB
- System type: 64-bit operating system, x64-based processor
- GPU: NVIDIA GeForce RTX 3070 Ti, Driver version: 527.37, 8 GB dedicated video RAM
- 3D Slicer 5.2.2
- LungCTAnalyzer 2.65
- TotalSegmentator 1.5.3
- Pytorch 2.0.0+cu118

The automated approach facilitated efficient and accurate segmentation of the lungs and lung pathologies, providing valuable insights into the disease progression and aiding in diagnosis and treatment planning.

Statistics

The statistical analysis was conducted using R version 4.2.3 and RStudio version 2023.03.0 Build 386. The ggplot2 package was used to generate figures.

The Shapiro-Wilk normality test showed that the % COVID affection was not normally distributed between lungs and lobes (p-value = 0.02375).

Thus, for group comparisons of COVID severity the Kruskal-Wallis test for group comparisons was used and the Wilcoxon rank sum test with Benjamini-Hochberg adjustment was added.

The reliability of the computed volume was evaluated using the intraclass correlation coefficient in the two-way random-effects model for intra- and inter-reader/retest assessments. Statistical significance was defined as a P value less than 0.05.

Results

Figure 1 illustrates a representative case of moderate COVID-19 manifestations, showcasing the automatic segmentation of lungs, lobes, and trachea without user intervention, using 3D Slicer's LungCTSegmenter. Figure 2 demonstrates the automatic volumetric analysis of the same patient, applying the previously described thresholds through the 3D Slicer LungCTAnalyzer.

Within the 78 patients, a strong correlation was observed between the analysis of Expert 1 and computer analysis ($R=0.86$, $p < 2.2e\text{-}16$, Figure 4)). Consequently, the median percentage of COVID-19-affected areas in each expert evaluation score exhibited significant differences ($p < 0.05$) from other scores, except for score classes 1 and 2, which were similar (Figure 5).

The correlation between expert and machine improved when using self-calibrated data (AIC Model 2, BIC Model 2), as evidenced by the AIC and BIC values (AIC 1 vs 2: 602.5 vs 586.4, BIC 1 vs 2: 609.5 vs. 593.5). The impact of data calibration is depicted in Figure 6.

With the participation of Expert 2, we observed a notable, statistically significant interobserver bias (Figure 8, stronger than anticipated), as evidenced by the Wilcoxon signed-rank test with continuity correction ($p < 0.05$).

No significant difference was found between the biological sexes (Figure 3).

Total lung affection is shown in Table 1, and there were no significant differences between the right and left lungs.

In regard to the lobes (Table 1), a higher degree of infiltration and collapse was observed in the left lower lobe compared to the upper lobe ($p < 0.05$). A similar pattern was found in the right lower lobes, with increased infiltration or collapse relative to the upper lobes ($p < 0.05$). No significant difference was detected in the COVID-19-related involvement when comparing the left and right lower lobes to each other. The right middle lobes demonstrated lower involvement compared to the right lower lobes ($p < 0.05$).

Upon examining the lung regions, significant differences in COVID-19 involvement were found when comparing the anterior and posterior halves of the lungs as the posterior regions showed higher COVID-19 involvement (Table 1). Comparing the upper and lower halves of both lungs, the lower halves of the lungs exhibited significantly greater COVID-19 involvement than the upper halves (Table 1).

It was particularly interesting that, according to computer analysis, patients who required admission to the intensive care unit during their inpatient treatment demonstrated significantly higher COVID-19 lung involvement (Figure 7), as compared to patients who could remain in general wards. Patients with >= 40% COVID-19 involvement (n=31) were predominantly treated in intensive care (n=24, 77%).

Discussion

The present study demonstrated the potential of 3D Slicer computer analysis as a reliable and reproducible tool for assessing lung involvement in patients with COVID-19. Our validation of computer analysis against expert radiological judgment revealed a high correlation between the two approaches in detecting COVID-19 affections. This finding is supported by a recent study [(15)] that suggests that computer analysis can effectively complement expert evaluation and contribute to more accurate and objective assessments of lung involvement.

In this study, the LungCTAnalyzer module uses a nnU-Net TotalSegmentator AI tool (11), which allowed autonomous computer analysis including lung lobes without human intervention. The use of AI-powered tools like the nnU-Net TotalSegmentator can provide several benefits, including reduced time spent on image analysis, increased consistency in assessments, and potentially improved patient outcomes due to faster and more accurate diagnosis. Furthermore, autonomous computer analysis could alleviate the workload of radiologists and healthcare professionals, especially during times of increased demand, such as the COVID-19 pandemic.

However, there are also potential dangers associated with relying solely on autonomous computer analysis, but the design of this study included AI only for the segmentation of lung masks and lung lobes.

The present study employs a two-way strategy for computer analysis of lung CT: First, anatomical structures are segmented using AI, and then the results are refined with conventional image processing methods, such as thresholding, smoothing, and volumetry. This approach is especially sound because autonomous deep-learning computer systems for detecting COVID-19 alone are on the horizon, but still have limitations (16), (17).

Our results have shown that automatic calibration of CT data is an elegant, efficient and feasible solution that may be particularly valuable for analyzing heterogeneous or artifact-laden datasets. The time required to perform a complete segmentation using 3D Slicer compared to manual delineation times (5 min vs. 2-3 min) still favors the human observer, however, it has to be noted that LungCTAnalyzer as well as its AI tool has not been optimized for speed yet. This, in combination with better hardware, will certainly reduce program execution times. In addition, the automated analysis could seamlessly be integrated into the data transfer process from the scanner, ensuring that it will have been automatically processed by the time the radiologist is ready to review the case. Thus in a practical setting, any potential delay becomes negligible.

Our results also highlighted the anatomical and regional differences in COVID-19 lung affections. We found a higher degree of infiltration and collapse in the lower lobes, the lower halves of the lungs, and the posterior lungs. These differences provide valuable insights into the distribution and extent of lung involvement in advanced COVID-19.

An important finding of our study is the potential of the 3D Slicer computer analysis method to predict the necessity for ICU treatment. The results indicated that patients with higher lung involvement (>40%) were almost exclusively treated in intensive care. This finding underscores the importance of understanding the extent of lung involvement to optimize resource allocation, particularly during a pandemic, when ICU resources may be limited.

However, it is important to note that there were seven patients with high pulmonary affections who did not require ICU admission. This phenomenon has been a common observation during the COVID-19 pandemic and highlights the multifactorial nature of the disease, in which deterioration of lung function may occur very late despite already significant pulmonary radiological affections (18), (19). This observation emphasizes the need for further investigation to better understand the factors that may

influence ICU admission requirements, such as comorbidities (20), patient age (21), and overall clinical presentation (22).

The limitations of the study should also be acknowledged. Our sample size was relatively small, which may limit the generalizability of our findings. Moreover, the study design was retrospective, and prospective studies with larger sample sizes are needed to confirm and expand upon these observations. Additionally, while the high correlation between expert and computer analysis is promising, further research is required to refine and optimize the 3D Slicer computer analysis tool, including the nnU-Net TotalSegmentator AI component, and validate its utility in different clinical settings. In addition, our method for calibration of the CT HU values could be improved, ideally through the use of calibration phantoms as part of the scanning protocol for any future prospective study. Similarly, our use of hard threshold values to define the areas of emphysema and otherwise characterize features could potentially be improved through the use of a soft threshold technique that might better quantify the volume of tissues in each class. We note though that in spite of these opportunities to improve the analysis we were able to find statistically significant correlates of disease severity in a relatively small sample size gives us confidence that the underlying approach shows promise.

A particular constraint of the initial study is that it included only a single radiological expert as a human control. Nevertheless, this limitation was an inherent component of the design in the preceding study. To address this, we introduced an additional reviewer who utilized the same scoring system (refer to Fig. 8). With the participation of two radiological experts, a notable, statistically significant interobserver bias was detected. This finding underscores the necessity for an automated, reproducible computer evaluation to mitigate such biases.

Another limitation of our study pertains to the variable "affected lung involvement", whose role as an independent predictor for ICU admission remains to be proven. In a more comprehensive study, this variable would ideally be incorporated into a multivariate regression analysis. This analysis would assess if "affected lung involvement" can hold its significance against well-established confounders, such as age and comorbidities. Unfortunately, the dataset used in our study does not include these variables, preventing us from performing this analysis at this time. Future prospective studies incorporating these data points will be necessary to conduct a more robust assessment.

Lastly, patterns, GGO, or “tinted signs” (23) may not be correctly detected by the threshold-based computer algorithms yet and would require further development of AI detection methods.

Despite these limitations, our study contributes valuable insights to the existing literature on lung involvement in COVID-19 and highlights the potential of 3D Slicer computer analysis as a reliable, reproducible, and complementary tool for expert radiological evaluation. The anatomical and regional differences in lung affections, as well as the potential to predict ICU treatment requirements, have important implications for clinical practice and resource allocation during a pandemic.

The availability of automatic volumetry of COVID-affections could also be extremely helpful during follow-up.

In this discussion of a science paper, it is important to emphasize that the methodology employed, using the 3D Slicer computer analysis, has broader applications beyond just COVID-19. This work demonstrates that a previously challenging image analysis problem, detailed segmentation of lung anatomy in patients with severe disease, is now routinely solvable using freely available software with reliability suitable to explore novel anatomical correlates of disease severity. The paper has effectively showcased how this approach can be used for the quantitative assessment of lung pathologies in the context of COVID-19. However, its utility extends to a wide range of pulmonary conditions, including fibrosis, emphysema, and other infectious lung diseases.

The versatility and potential of the 3D Slicer-based LungCTAnalyzer, alongside the nnU-Net TotalSegmentator AI component, make it a promising tool for future research and clinical practice. The fact that the software is open-source and freely available to researchers worldwide further bolsters its potential impact, as it encourages collaboration and continuous improvement within the scientific community.

As our methodology has proven effective in the present case study of COVID-19 and has also been used in the quantification of lung changes in chest CT of patients with mutations of the novel coronavirus 2 with success (24), future research should explore its applications in the context of other lung pathologies, both infectious and non-infectious. This would not only provide additional insights into the value and limitations of this approach but also help optimize patient care and outcomes across a variety of pulmonary conditions. By doing so, the scientific community can work together to refine and expand the use of AI-powered tools, ensuring that they complement and enhance expert human judgment in the assessment and management of lung diseases.

Conclusion

In conclusion, our study demonstrates the distribution and extent of lung involvement in patients with COVID-19 and highlights the potential association between the degree of lung involvement and the need

for ICU admission. A high correlation was observed between computer detection of COVID-19 affections and expert rating by a radiological expert, suggesting that computer analysis may be a valuable tool for evaluating lung involvement in clinical practice. This information can contribute to more informed clinical decision-making and resource allocation during current and future pandemics. Our findings provide a foundation for further research with larger sample sizes to validate and expand upon these observations. Ultimately, enhancing our understanding of lung involvement in COVID-19 and refining the tools used to assess this involvement can improve patient care and outcomes during global health crises.

Declarations

Acknowledgments

Funding: This research was supported by

rk: NIH grants: P41 EB015902, P41EB028741, R01 CA235589. National Cancer Data Ecosystem, Task Order No. 413 HHSN26110071 under Contract No. HHSN261201500003l

Footnote

Conflicts of Interest: All authors have completed the ICMJE uniform disclosure form (available at https://qims. amegroups.com/article/view/10.21037/qims-22-718/coif). The authors have no conflicts of interest to declare.

Ethical Statement: The authors are accountable for all aspects of the work in ensuring that questions related to the accuracy or integrity of any part of the work are appropriately investigated and resolved. The study was conducted according to the guidelines of the Declaration of Helsinki (as revised in 2013), and approved by the Ethics Committee of Cologne University (No. 20-1676). The requirement for informed consent was waived, due to the study was a retrospective study without any contact with patients. All the imaging data were anonymized. The study process did not reveal the patients' private information, increase the patient's pain, or cause any damage.

LLM[1] Statement: As the primary author is a non-native English speaker, he utilized the GPT-4 model as an editing tool during the creation of this article to:

- review and amend spelling and grammatical errors
- ensure linguistic consistency and coherence
- test and fine-tune the wording of the article
- standardize the format of the Annotated Bibliography

_–––

[1]LLM: A Large Language Model is an advanced machine learning model that is capable of processing vast amounts of language data and generating human-like responses to queries.

References

1. Li Q, Guan X, Wu P, Wang X, Zhou L, Tong Y, et al. Early Transmission Dynamics in Wuhan, China, of Novel Coronavirus-Infected Pneumonia. N Engl J Med. 2020 Mar 26;382(13):1199–207.

2. Wu F, Zhao S, Yu B, Chen YM, Wang W, Song ZG, et al. A new coronavirus associated with human respiratory disease in China. Nature. 2020 Mar;579(7798):265–9.

3. Dong E, Du H, Gardner L. An interactive web-based dashboard to track COVID-19 in real time. Lancet Infect Dis. 2020 May 1;20(5):533–4.

4. Ai T, Yang Z, Hou H, Zhan C, Chen C, Lv W, et al. Correlation of Chest CT and RT-PCR Testing for Coronavirus Disease 2019 (COVID-19) in China: A Report of 1014 Cases. Radiology. 2020 Aug;296(2):E32–40.

5. Fang Y, Zhang H, Xie J, Lin M, Ying L, Pang P, et al. Sensitivity of Chest CT for COVID-19: Comparison to RT-PCR. Radiology. 2020 Aug;296(2):E115–7.

6. Pan F, Ye T, Sun P, Gui S, Liang B, Li L, et al. Time Course of Lung Changes at Chest CT during Recovery from Coronavirus Disease 2019 (COVID-19). Radiology. 2020 Jun;295(3):715–21.

7. Rudolf Bumm, Andras Lasso. Lung CT Analyzer on GitHub [Internet]. Lung CT Analyzer. Available from: https://github.com/rbumm/SlicerLungCTAnalyzer

8. Kikinis R, Pieper SD, Vosburgh KG. 3D Slicer: A Platform for Subject-Specific Image Analysis, Visualization, and Clinical Support. In: Jolesz FA, editor. Intraoperative Imaging and Image-Guided Therapy [Internet]. New York, NY: Springer; 2014 [cited 2021 Apr 13]. p. 277–89. Available from: https://doi.org/10.1007/978-1-4614-7657-3_19

9. Kikinis R, Pieper S. 3D Slicer as a tool for interactive brain tumor segmentation. Annu Int Conf IEEE Eng Med Biol Soc IEEE Eng Med Biol Soc Annu Int Conf. 2011;2011:6982–4.

10. Zaffino P, Marzullo A, Moccia S, Calimeri F, De Momi E, Bertucci B, et al. An Open-Source COVID-19 CT Dataset with Automatic Lung Tissue Classification for Radiomics. Bioeng Basel Switz. 2021 Feb

16;8(2).

11. Jakob Wasserthal MM Hanns Christian Breit, Joshy Cyriac, Shan Yang, Martin Segeroth. TotalSegmentator: robust segmentation of 104 anatomical structures in CT images. arXiv:220805868 [Internet]. Available from: https://arxiv.org/abs/2208.05868

12. Harris CR, Millman KJ, van der Walt SJ, Gommers R, Virtanen P, Cournapeau D, et al. Array programming with NumPy. Nature. 2020 Sep;585(7825):357–62.

13. Lasso A. TotalSegmentator extension for 3D Slicer [Internet]. 2023 [cited 2023 May 6]. Available from: https://github.com/lassoan/SlicerTotalSegmentator

14. Isensee F, Jaeger PF, Kohl SAA, Petersen J, Maier-Hein KH. nnU-Net: a self-configuring method for deep learning-based biomedical image segmentation. Nat Methods. 2021 Feb;18(2):203–11.

15. Risoli C, Nicolò M, Colombi D, Moia M, Rapacioli F, Anselmi P, et al. Different Lung Parenchyma Quantification Using Dissimilar Segmentation Software: A Multi-Center Study for COVID-19 Patients. Diagnostics. 2022 Jun;12(6):1501.

16. Aslani S, Jacob J. Utilisation of deep learning for COVID-19 diagnosis. Clin Radiol. 2023 Feb;78(2):150–7.

17. Li Z, Zhong Z, Li Y, Zhang T, Gao L, Jin D, et al. From community-acquired pneumonia to COVID-19: a deep learning-based method for quantitative analysis of COVID-19 on thick-section CT scans. Eur Radiol. 2020 Dec;30(12):6828–37.

18. Zhou F, Yu T, Du R, Fan G, Liu Y, Liu Z, et al. Clinical course and risk factors for mortality of adult inpatients with COVID-19 in Wuhan, China: a retrospective cohort study. The Lancet. 2020 Mar 28;395(10229):1054–62.

19. Guan W jie, Ni Z yi, Hu Y, Liang W hua, Ou C quan, He J xing, et al. Clinical Characteristics of Coronavirus Disease 2019 in China. N Engl J Med. 2020 Apr 30;382(18):1708–20.

20. Yang X, Yu Y, Xu J, Shu H, Xia J, Liu H, et al. Clinical course and outcomes of critically ill patients with SARS-CoV-2 pneumonia in Wuhan, China: a single-centered, retrospective, observational study. Lancet Respir Med. 2020 May 1;8(5):475–81.

21. Dowd JB, Andriano L, Brazel DM, Rotondi V, Block P, Ding X, et al. Demographic science aids in understanding the spread and fatality rates of COVID-19. Proc Natl Acad Sci. 2020 May 5;117(18):9696–8.

22. Petrilli CM, Jones SA, Yang J, Rajagopalan H, O'Donnell L, Chernyak Y, et al. Factors associated with hospital admission and critical illness among 5279 people with coronavirus disease 2019 in New York City: prospective cohort study. BMJ. 2020 May 22;369:m1966.

23. Martini K, Larici AR, Revel MP, Ghaye B, Sverzellati N, Parkar AP, et al. COVID-19 pneumonia imaging follow-up: when and how? A proposition from ESTI and ESR. Eur Radiol. 2022;32(4):2639–49.

24. Kottlors J, Fervers P, Geißen S, Gertz RJ, Bremm J, Rinneburger M, et al. Morphological appearance of the B.1.1.7 mutation of the novel coronavirus 2 (SARS-CoV-2) in chest CT. Quant Imaging Med Surg. 2023 Feb 1;13(2):1058–70.

Cite this article as Bumm R, Zaffino P, Lasso A, Estépar RSJ, Pieper S, Wasserthal J, Spadea MF, Latshang T, Kawel-Böhm N, Wäckerlin A, Werner R, Hässig G, Furrer M, and Kikinis R; From Voxels to Prognosis: AI-Driven, quantitative Chest CT Analysis Forecasts ICU Requirements in 78 COVID-19 Cases

Tables

Structure	Mean	Median	SD	q1	q3	iqr	comparison	p
Total lungs	35.2	35	18.8	18	49	30		
Right lung	35.5	34	19.0	19	48	29	RL vs LL	n.s.
Left lung	35.9	36	19.0	18	49	31	LL vs RL	n.s.
Right upper lobe	30.6	26	19.7	12.5	42	29	RUL vs ML	n.s.
Right middle lobe	28.1	21	19.5	11	44	32	ML vs RUL	n.s.
Right lower lobe	44.8	47	22.4	27	60	33	RLL vs RUL RLL vs ML	p = 0.00012 p = 2.8e-05
Left upper lobe	29.7	28	18.2	13	41	28	LUL vs LLL	p = 0.00011
Left lower lobe	44.4	43	23.0	23	62	39	LLL vs LUL	p = 0.00011
Anterior	36.0	35	19.9	19	51	32	A vs P	p = 0.00019
Posterior	41.2	42	21.2	21	58	37	P vs A	p = 0.00019
Upper half	31.4	29.5	18.6	14.2	44	13	UH vs LH	p = 0.02001
Lower half	39.2	39.5	20.2	20.2	54	34	LH vs UH	p = 0.02001

Table 1 Percentage of COVID-affected lung tissue according to anatomical structures and regions. Differences were evaluated with the Kruskal-Wallis test for group comparisons and the Wilcoxon rank sum test with Benjamini-Hochberg adjustment. RL = right lung, LL = left lung, RUL = right upper lobe, ML = right middle lobe, RLL = right lower lobe. Taking into account both lungs: A = anterior half, P = posterior half, UH = upper half, LH = lower half

Figures

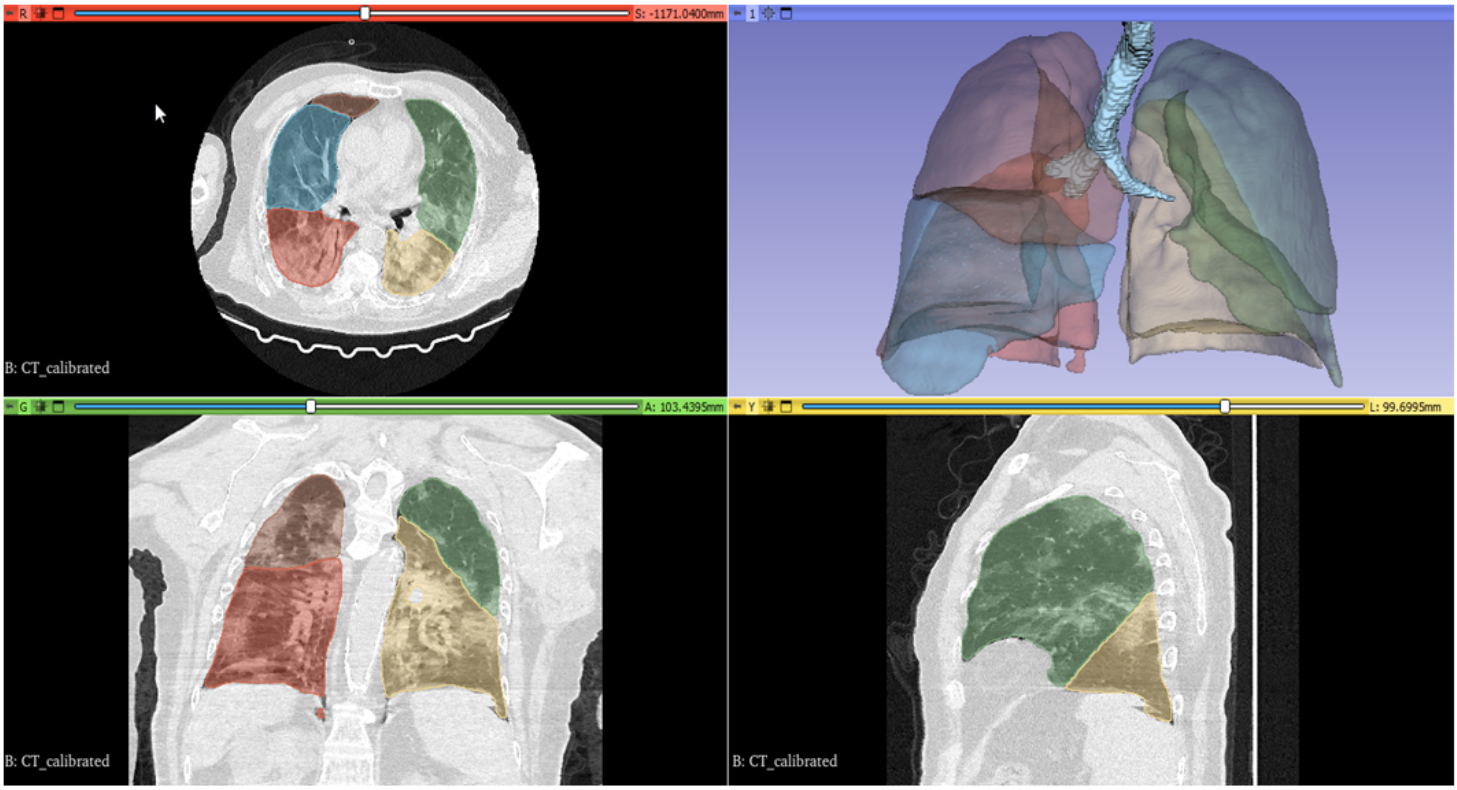

Figure 1

Case example: Patient #78 Lung CT Segmentation of trachea, lungs, and lobes in calibrated scalar volume

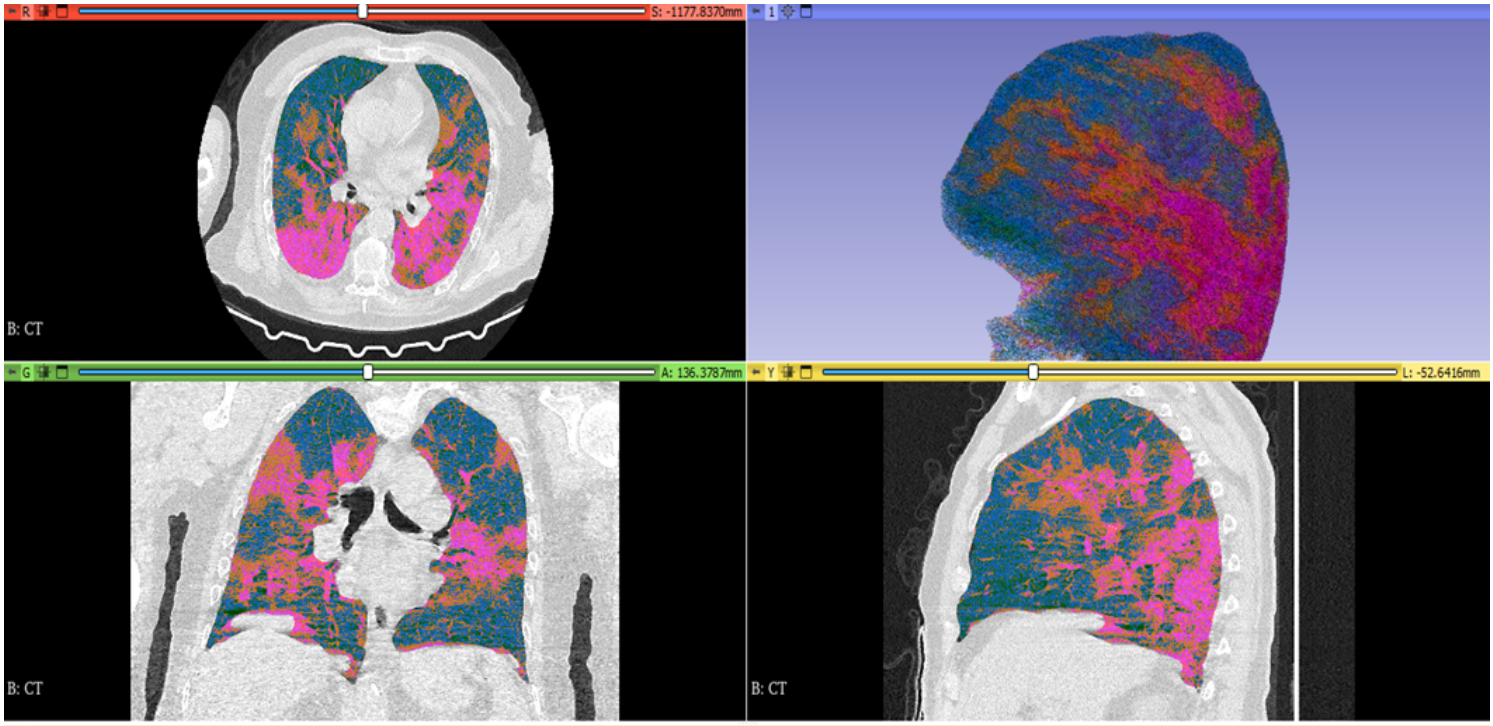

	A	B	C	D	E	F	G	H	I	J	K	L
1	**Lung area**	**Total (ml)**	**Inflated (ml)**	**Inflated (%)**	**Emphysema (ml)**	**Emphysema (%)**	**Infiltrated (ml)**	**Infiltrated (%)**	**Collapsed (ml)**	**Collapsed (%)**	**Affected (ml)**	**Affected (%)**
2	Total lungs	3399.16	1218.12	36	372.903	11	1186.72	34.9	621.427	18.3	1808.14	53
3	Right lung	1820.37	837.83	46	204.779	11.2	635.118	34.9	347.424	19.1	982.542	54
4	Left lung	1578.79	789.846	50	168.124	10.6	551.598	34.9	274.003	17.4	825.601	52

Figure 2

Case example: Same Patient #78 after Lung CT Analysis of calibrated scalar volume with signs of severe SARS-CoV-2 affection (> 50 % in both lungs). Green: Emphysema. Blue: normal lung. Orange: Infiltration. Pink: Collapse. Orange + Pink = Affected. Red: Vessels.

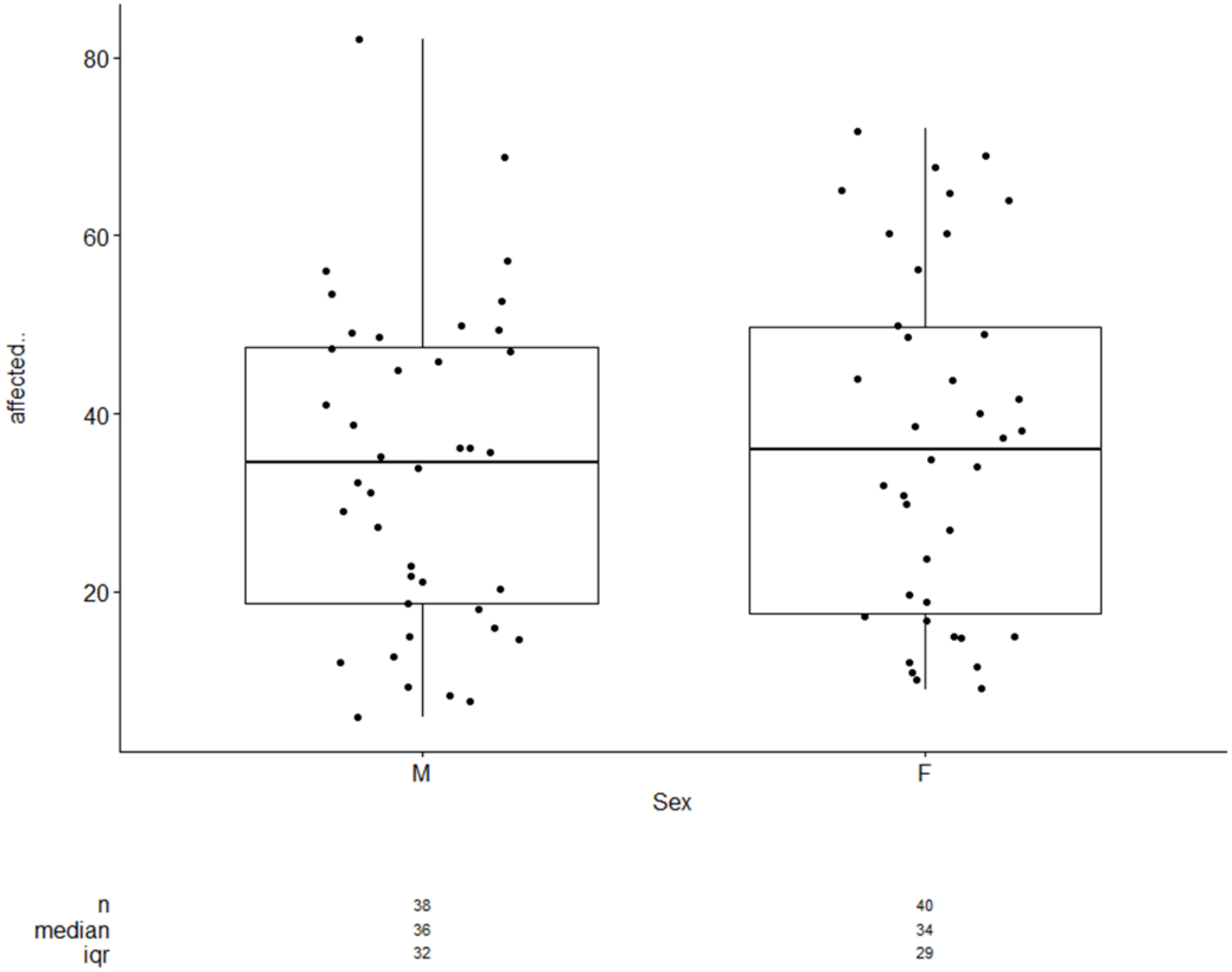

Figure 3

This Box and Whisker plot shows the even distribution of COVID affecting lung CT with no difference between biological sexes.

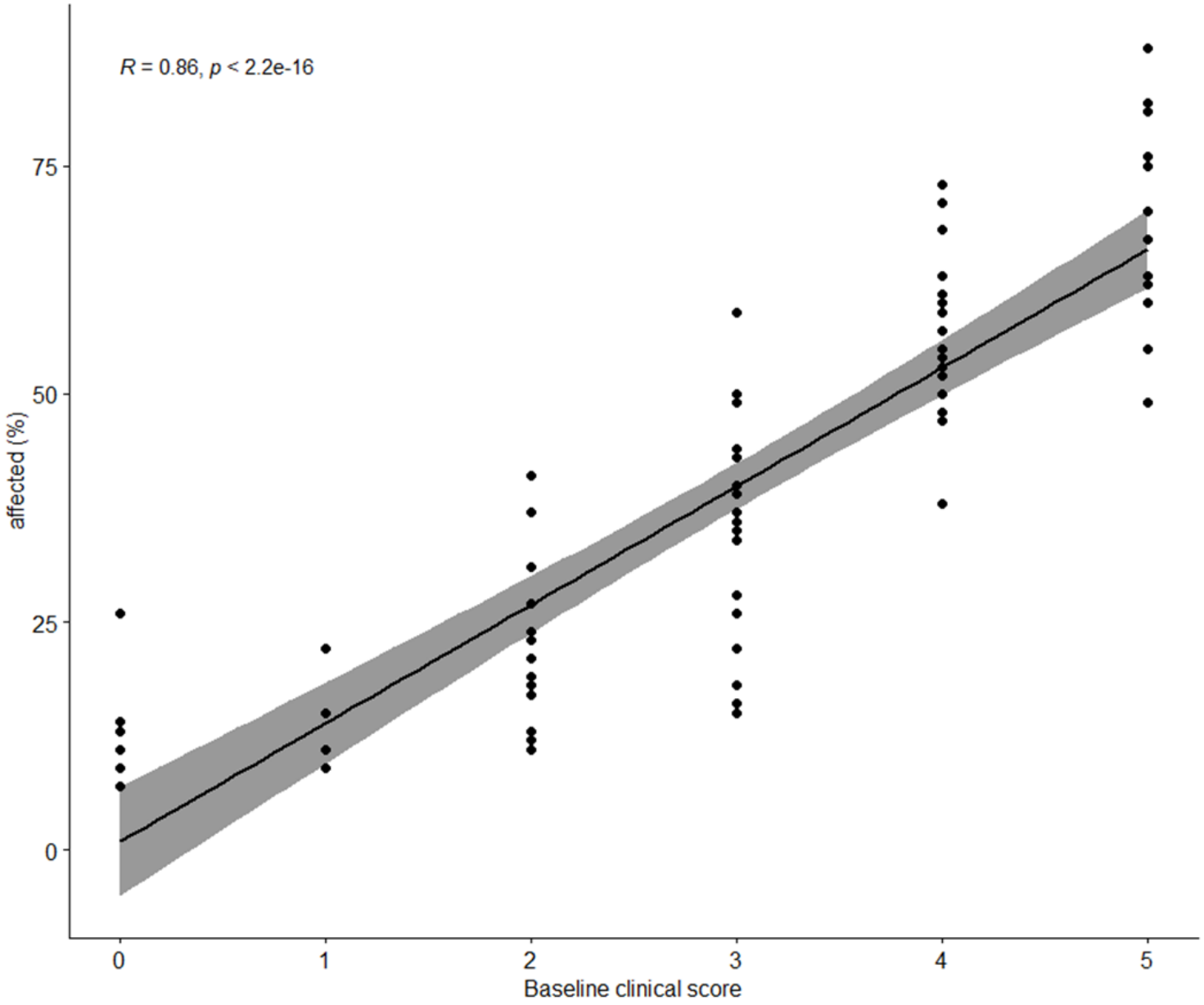

Figure 4

Correlation between baseline clinical score (by an expert radiologist) and percentage of COVID-affected lung derived by f automatic computer analysis (R = 0.86, p < 2.2e-16)

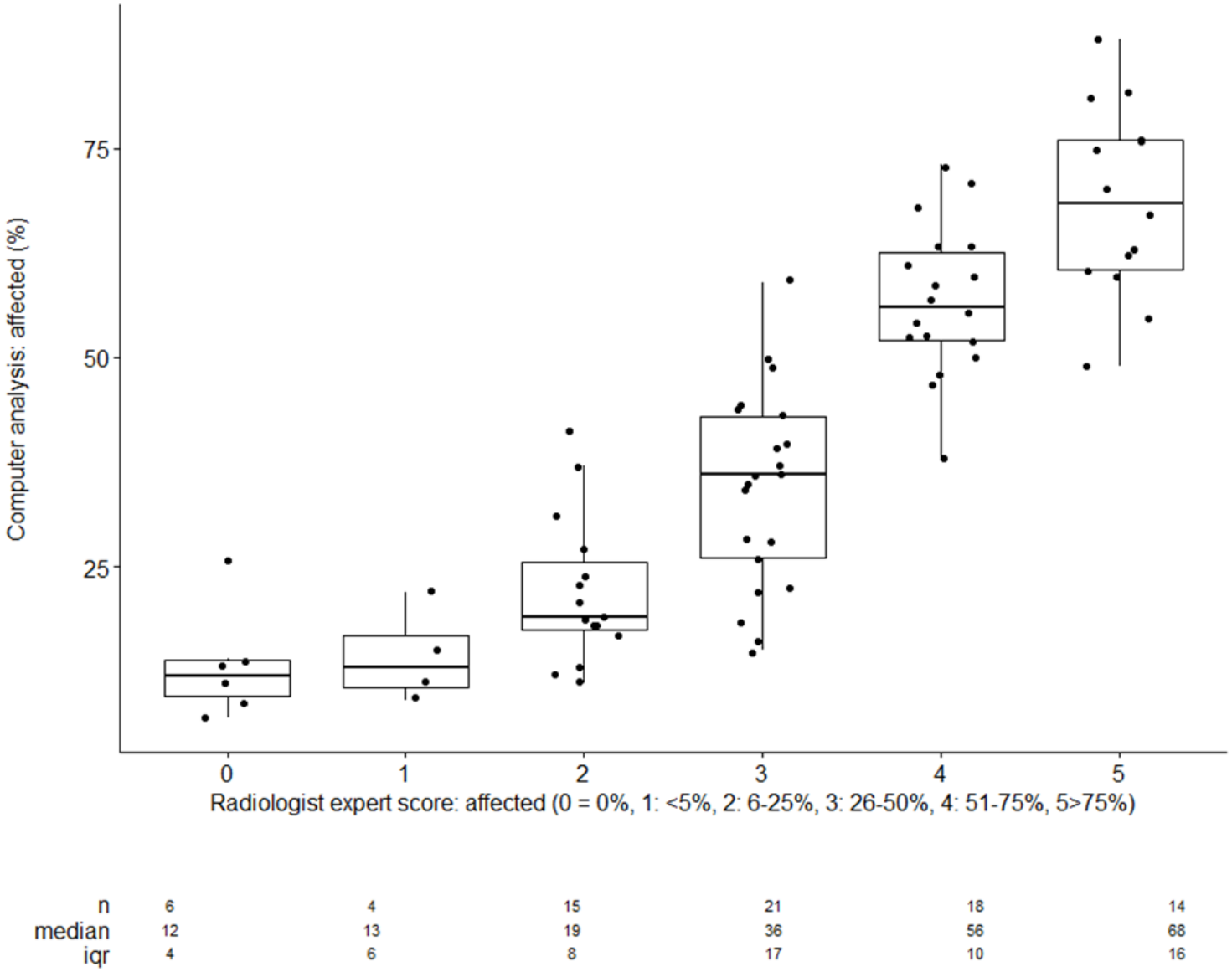

Figure 5

This box-and-whisker Plot was created to visualize the distribution of percentages of COVID-affection in each expert score group. All scores showed significantly different values with the exception of score 1 vs. 2 (* = $p < 0.05$)

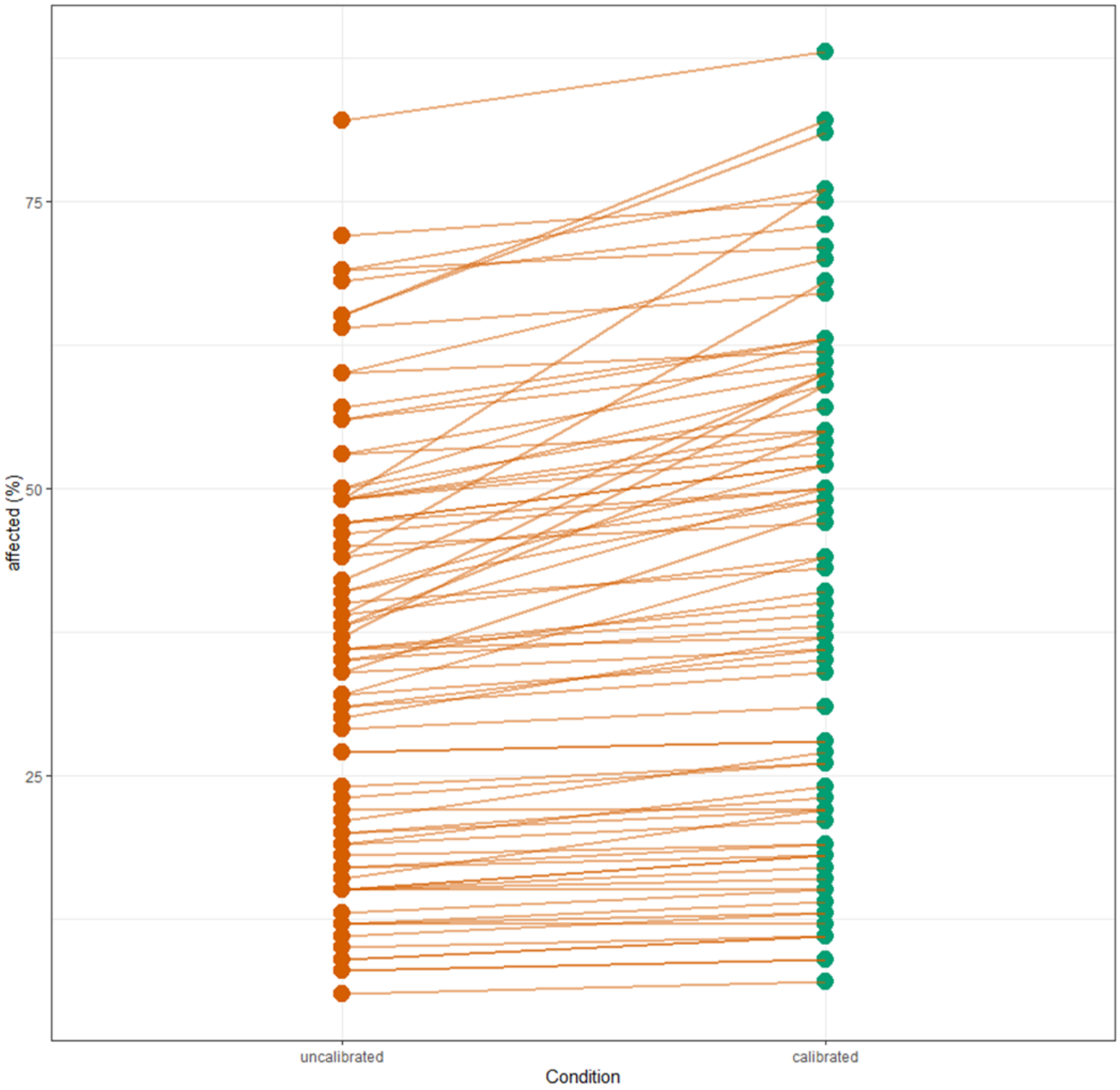

Figure 6

This scatter plot shows the percentage of COVID-affected samples under two conditions: uncalibrated and calibrated. The data points are color-coded based on their respective conditions, with green representing the calibrated condition and orange representing the uncalibrated condition. Additionally, lines connect the data points within each pairing, illustrating the change in affected percentage between the two conditions. The plot employs a white background theme, with the x-axis labeled "Condition" and the y-axis labeled "Affected (%)". The x-axis displays the two conditions in a discrete manner, with the order of the categories set manually. The color legend is omitted from the plot for clarity.

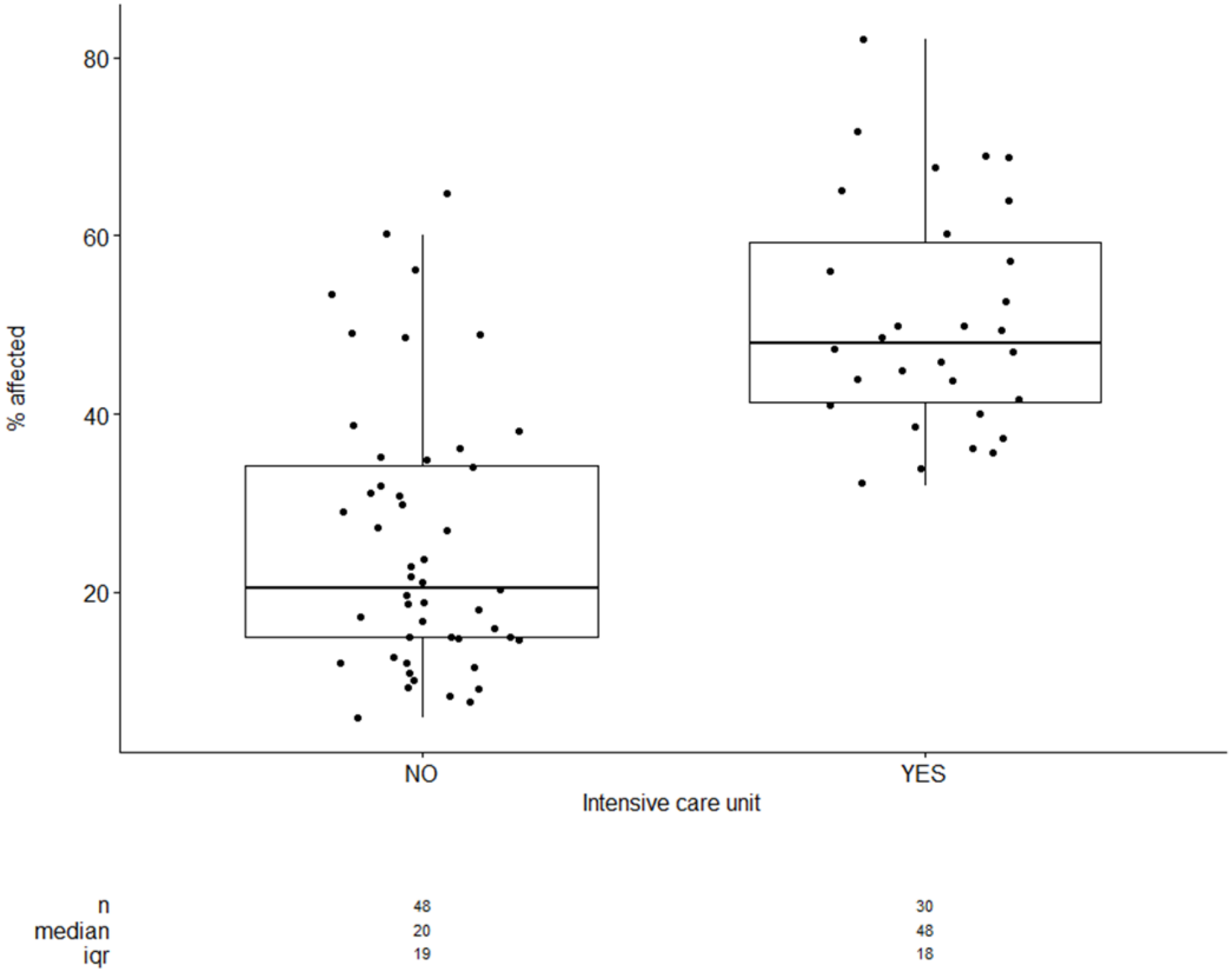

Figure 7

This box-and-whisker plot shows the distribution of the percentage of affected samples among patients needing or not to be admitted to the ICU. This is represented on the x-axis, while the y-axis displays the percentage of COVID-affected lung volume. Within each ICU category, a boxplot summarizes the median, quartiles, and outliers of the affected percentage. Jittered individual data points are overlaid on the boxplots, visually representing the underlying data distribution. Patients who needed ICU support had significantly higher percentages of COVID alterations in both lungs. ($p < 0.05$)

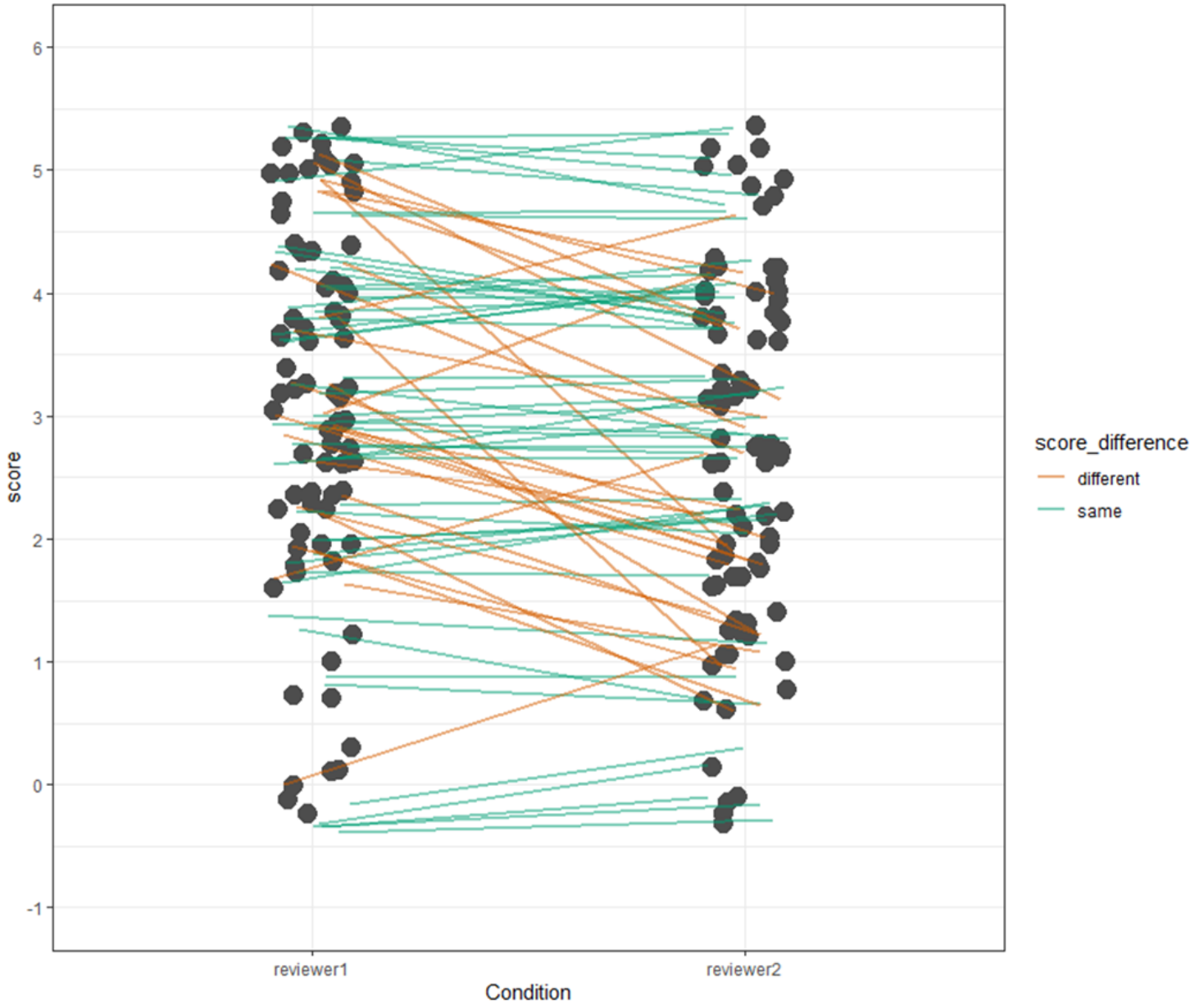

Figure 8

This scatter plot shows the distribution of scores between the two reviewers. Jittered individual data points are above each reviewer and identical scores are represented by green, diverging scores by orange lines (31 of 81, 38%). The second reviewer felt unable to score and excluded 3 CT scans (“NA”: 1 pneumothorax, 2 preexistent lung diseases) In the Wilcoxon signed rank test with continuity correction there was a statistically significant interobserver bias (V = 356, p-value = 0.0001666).